JVI Journals.ASM.org

Reselection of a Genomic Upstream Open Reading Frame in Mouse Hepatitis Coronavirus 5′-Untranslated-Region Mutants

Hung-Yi Wu,[a]* Bo-Jhih Guan,[b]* Yu-Pin Su,[a] Yi-Hsin Fan,[a] David A. Brian[a,b]

Departments of Biomedical and Diagnostic Sciences[a] and Microbiology,[b] University of Tennessee, College of Veterinary Medicine, Knoxville, Tennessee, USA

An AUG-initiated upstream open reading frame (uORF) encoding a potential polypeptide of 3 to 13 amino acids (aa) is found within the 5′ untranslated region (UTR) of >75% of coronavirus genomes based on 38 reference strains. Potential CUG-initiated uORFs are also found in many strains. The AUG-initiated uORF is presumably translated following genomic 5′-end cap-dependent ribosomal scanning, but its function is unknown. Here, in a reverse-genetics study with mouse hepatitis coronavirus, the following were observed. (i) When the uORF AUG-initiating codon was replaced with a UAG stop codon along with a U112A mutation to maintain a uORF-harboring stem-loop 4 structure, an unimpaired virus with wild-type (WT) growth kinetics was recovered. However, reversion was found at all mutated sites within five virus passages. (ii) When the uORF was fused with genomic (main) ORF1 by converting three in-frame stop codons to nonstop codons, a uORF-ORF1 fusion protein was made, and virus replicated at WT levels. However, a frameshifting G insertion at virus passage 7 established a slightly 5′-extended original uORF. (iii) When uAUG-eliminating deletions of 20, 30, or 51 nucleotides (nt) were made within stem-loop 4, viable but debilitated virus was recovered. However, a C80U mutation in the first mutant and an A77G mutation in the second appeared by passage 10, which generated alternate uORFs that correlated with restored WT growth kinetics. *In vitro*, the uORF-disrupting nondeletion mutants showed enhanced translation of the downstream ORF1 compared with the WT. These results together suggest that the uORF represses ORF1 translation yet plays a beneficial but nonessential role in coronavirus replication in cell culture.

Upstream open reading frames (uORFs) are present in ~40% of eukaryotic mRNAs (1, 2) and are found in the mRNAs of many viruses that infect eukaryotes (3–6). The function of the uORF is not known in a majority of cases, but in many mRNAs, it has been shown to cause repression of translation of the downstream (main) ORF (1, 2), usually following 5′-cap-dependent translation of the uORF. In other cases, 5′-cap-dependent translation of the uORF enhances translation of the main ORF by various mechanisms (1, 2, 4, 7–11). Some plant (12) and animal (13–15) viruses that have a positive-strand (mRNA-like) genome which undergoes necessary 5′-cap-dependent translation prior to viral genome replication in the cytoplasm also have a (usually single) short uORF. It might be expected that in these cases, the uORF in the genome would be a regulator of not only translation but also virus replication and perhaps also virus-induced pathogenesis. A single AUG-initiated uORF is found in the genomes of arteriviruses (13, 14, 16) and most coronaviruses (17; this study), two families of animal positive-strand RNA viruses in the order *Nidovirales* (18). The role of the uORF in these viruses has undergone limited study.

Arteriviruses and coronaviruses share features with regard to genome structure and replication (Fig. 1A shows a schematic of the mouse hepatitis coronavirus [MHV] genome and subgenomic mRNAs [sgmRNAs]) (18). The genomes are long (~12 kb for arteriviruses and ~30 kb for coronaviruses), single-strand molecules that are 5′ capped and 3′ polyadenylated and undergo replication via a full-length minus-strand (antigenome) intermediate in the cytoplasm, although to date, only coronaviruses have been shown to encode an N^7-methyltransferase and a 2′-*O*-methyltransferase needed for methylated cap formation (18–24). A guanylyltransferase has not yet been characterized for either virus. Both arteriviruses and coronaviruses are presumed to use 5′-cap-dependent, 5′-terminal 40S ribosomal entry with subsequent ribosomal scanning for translation of the genome. Both make a 3′-coterminal nested set of (five to nine) sgmRNAs, each of which has a 5′-terminal leader identical to the single-copy leader on the genome (16, 25). It is thought that for viruses in both families, the leader on sgmRNAs is acquired during minus-strand synthesis when the templates for the sgmRNAs are made (26, 27). The mechanism for leader acquisition is thought to be a template switching of the RNA-dependent RNA polymerase (RdRp) during minus-strand synthesis from pentameric (arteriviruses) or heptameric (coronaviruses) donor signaling sequences at intergenic regions within the genome (often called the transcription regulatory sequence [TRS]) to an equivalent acceptor sequence near the 3′ end of the 5′-terminal leader on the genome (26–29). With respect to the 5′ untranslated region (UTR) and AUG-initiated uORF arrangement, however, arteriviruses and coronaviruses differ in the following ways. (i) In arteriviruses, although the genomic 5′-UTR length is similar to the shortest in coronaviruses (~200 to 225 nucleotides [nt] for arteriviruses versus ~200 to 500 nt for coronaviruses), the leader is longer (~200 nt for arteriviruses versus 65 to 90 nt for coronaviruses) (16, 17). (ii) In arteriviruses, the uORF maps within the leader, whereas in coronaviruses, the uORF maps just downstream of the genomic leader. As a conse-

Received 26 September 2013 **Accepted** 25 October 2013

Published ahead of print 30 October 2013

Address correspondence to David A. Brian, dbrian@utk.edu.

* Present address: Hung-Yi Wu, Institute of Pathobiology, College of Veterinary Medicine, National Chung-Hsing University, Taichung, Taiwan; Bo-Jhih Guan, Department of Pharmacology, School of Medicine, Case Western Reserve University, Cleveland, Ohio, USA.

H.-Y.W. and B-J.G. contributed equally to this article.

doi:10.1128/JVI.02831-13

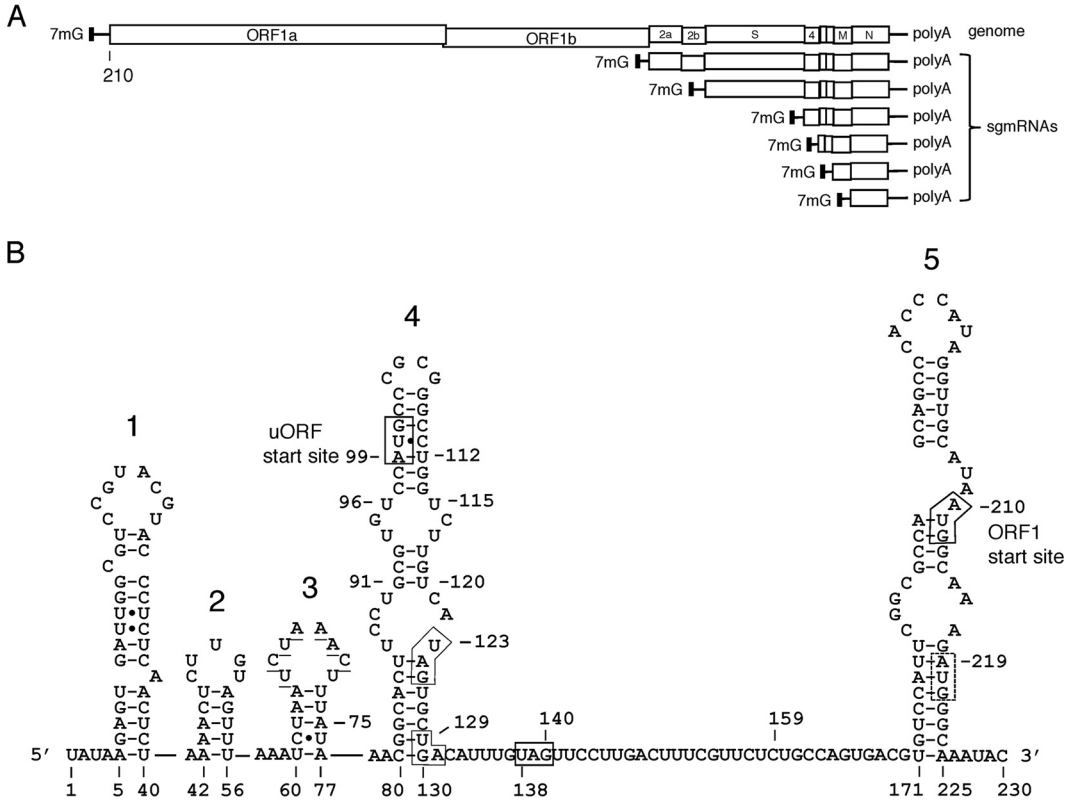

FIG 1 MHV genomic 5′ UTR. (A) MHV genome and subgenomic mRNAs. A uORF is found within the 5′ UTR of the genome but not sgmRNAs. ORF1 is translated from the genome beginning at nt 210 to produce a polyprotein that is co- and posttranslationally processed into 16 replicase-related nonstructural proteins. The 3′ nested set of sgmRNAs is translated to produce the virion structural proteins. A pseudoknot-induced −1 frameshifting event at the ORF1a/1b junction during translation maintains an optimal ratio of ORF1a and ORF1b proteins for virus replication. The filled bar at the 5′ terminus of each mRNA species represents the common leader that is encoded only at the genomic 5′ end. (B) RNA structures in the MHV genomic 5′ UTR. Shown are stem-loops 1 through 5 identified by bioinformatic, genetic, and physical structure analyses. Nucleotides 140 through 170 form a long-range RNA-RNA interaction with downstream nt 332 through 363 (not shown). The underlined heptameric sequence UCUAAAC in stem-loop 3 at the 3′ terminus of the leader is the core RdRp template-switching signal that directs leader acquisition on MHV sgmRNAs. Boxes identify the uORF start codon (nt 99), the genomic ORF1 start codon (nt 210), and a second nearby potential alternate ORF1 start codon (nt 219) as well as three in-frame stop codons for the uORF. Positions used for deleting regions of stem-loop 4 (nt 96 through 115, 91 through 120, 80 through 130, and 75 through 138) are identified. Potential CUG-initiated translation start sites in frame with the uORF and ORF1 are found beginning at nt 111 and 159.

quence, the uORF is found on the genome and on each sgmRNA in arteriviruses, whereas in coronaviruses, the uORF, with very few exceptions (30), is found only on the genome (Table 1).

The role that the uORF plays in nidoviruses has been examined most closely in arteriviruses (13, 14). When the AUG start codon for the uORF in equine arteritis virus, which is in a suboptimal Kozak context for translation, was changed to an AGG nonstart codon by mutation in a reverse-genetics analysis, or when the Kozak context was made optimal, the resulting virus plaque size was smaller than that of the wild type (WT), and growth kinetics were found to be impaired (13). In this case, reselection of a uORF start codon in its original suboptimal context was found upon virus passaging in cell culture. In another similar reverse-genetics study with the same virus, growth impairment was not observed with an AUG→AGG mutation, but reversion to a WT AUG was found upon virus passaging (14). These studies together would indicate that the uORF plays a beneficial role in arterivirus survival in cell culture, but the contribution of the uORF to fitness has not been characterized. In betacoronaviruses, features of the uORF in MHV were learned when the *cis*-acting properties of the stem-loop 4 structure, which harbors the uORF, were investigated by reverse genetics (31). In a previous study by Yang et al. (31), it was found that a 30-nt deletion of a distal portion of stem-loop 4 (nt 91 through 120), which removed almost all of the uORF, surprisingly remained viable although mildly debilitated, whereas deletion of a predicted 64-nt-long version of a complete stem-loop 4 (nt 75 through 138) was lethal. It was also shown that mutation of the uORF AUG to a nonstart AGG codon was detrimental to virus growth in cell culture. In studies described here using the same strain of MHV (MHV-A59), carried out largely concurrently with those of Yang et al. (31) and with some of the same mutations, we confirm the discovery of Yang et al. regarding the behavior of deleted features of stem-loop 4 but also extend these findings by describing the phenomenon of uORF reselection and demonstrating that the deletion of a predicted 51-nt-long shorter version of a complete stem-loop 4 (nt 80 through 130) is viable.

Here, with a reverse-genetics system for MHV, three different experimental approaches were used to disrupt the AUG-initiated uORF and test for the tendency of the virus to restore an intact uORF, by reversion or by compensatory changes, upon passaging of progeny virus. In all three approaches, restoration of a uORF was found in most mutants within 8 to 10 passages, although the

TABLE 1 Predicted coronavirus AUG-initiated uORFs in 38 GenBank reference strains

Virus[a]	5′ UTR (nt)	Predicted AUG-initiated uORF and ORF1 start codons within the Kozak context[b]	uORF peptides	GenBank accession no. of reference sequence
Alphacoronavirus				
TGEV-Purdue	314	5′. . .CTTTCTA^{117}TGAAATCATAG^{128}. . .AGGAGAA^{315}TGA. . .	MSK	DQ811788
FCoV	311	5′. . .CTCTCTA^{117}TGAAACCATAG^{128}. . .AGGAGAA^{312}TGA. . .	MKP	NC_002306
RhBtCoV-HKU2	296	5′. . .TTGTGTA^{98}TGCTACGCATGCACAATT^{116}AGA^{119}TGTGTATTT^{128}GA. . .TGCACAA^{297}TGT. . .	MLRMHN, MCI	NC_009988
HCoV-NL63	288	5′. . .TTTGTTA^{101}TGGCAGTCCTAGTGT^{114}AA. . .CTAACCA^{289}TGT. . .	MAVLV	NC_005831
HCoV-229E	292	5′. . .TTTGCTA^{86}TGGCCGGCATCTTTGATGCTGGAGTCGTAGTGT^{119}AA. . .TTCCTAA^{293}TGG. . .	MAGIFDAGVVV	NC_002645
ScBtCoV-512	293	5′. . .GCACACA^{97}TGTCTATGTGTGCTGAAGTGAAATTGGAATTTCGCT^{133}AG. . .TTAGCTA^{294}TGG. . .	MSMCAEVKLEFR	NC_009657
PEDV	296	5′. . .GGCCGCA^{99}TGTTCATGCTGCTGGAAGCTGGCGTGGAATTTCATT^{135}AG. . .CCGGCTA^{297}TGG. . .	MMFMLLEAGVEFH	NC_003436
MiBtCoV-1A	271	5′. . .TGCCATA^{87}TGTTTATGGCTAATT^{102}GA. . .	MFMAN	NC_010437
		TCGTGCA^{146}TGTCGCCAGTCCCTCCTTTCAGTTCCGTCTGTT^{177}AG. . .GCAGGTA^{272}TGT. . .	MSPVPPFSSVC	
MiBtCoV-1B	272	5′. . .TGCCATA^{88}TGTTTATGGCGAATT^{103}GA. . .	MFMAN	NC_010436
		TCGTGCA^{147}TGTCACTAGTCCCTCCTTCCAGTTCCGTCTGGT^{180}AG. . .GCAGGTA^{273}TGC. . .	MSLVPPSSSVW	
MiBtCoV-HKU8	268	5′. . .ACTTGTA^{94}TGGCGGATT^{103}GA. . .GTCGCTA^{269}TGG. . .	MAD	NC_010438
RoBtCoV-HKU10	302	5′-ACA^{3}TG(72 nt)T^{88}AA	25 aa	NC_018871
		GCACACA^{104}TGTTCGCATGTGTTTGCGTATGGTGCAATT^{134}GA	MFACVCVWCN	
		GTTCGCA^{112}TGTGTTTGCGTATGGTGCAATTGAAATTTCATT^{145}AG. . .TGCCCAA^{303}TGG	MCLRMVQLKFH	
Betacoronavirus A				
BCoV-Mebus	210	5′. . .TATTCTA^{100}TGCTTGTGGGCGTAGATTTTTCAT^{124}AG. . .GTCACAA^{211}TGT. . .	MPVGVDFS	U00735
HCoV-OC43	210	5′. . .TAATCTA^{100}TGCTTGTGGGCGTAGATTTTTCAT^{124}AG. . .GTCACAA^{211}TGT. . .	MLVGVDFS	NC_005147
PHEV-VW572	210	5′. . .TAGTCTA^{100}TGCTTGTGGGCGTAGATTTTTCAT^{124}AG. . .GTCACAA^{211}TGT. . .	MLVGVDFS	NC_007732
ECoV	208	5′. . .TAATCTA^{99}TGCTTGCGAGCTTAGACTTTTCAT^{121}AG. . .GTCACAA^{209}TGG. . .	MLASLDFS	NC_010327
MHV-A59	209	5′. . .GTGTCCA^{99}TGCCCGCGGGCCTGGTCTTGTCAT^{123}AG. . .TGCATAA^{210}TGG. . .	MPAGLVLS	NC_001846
MHV-JHM	214	5′. . .GTGTCCA^{104}TGCCCGTGGGCCTGGTCTTGTCAT^{128}AG. . .TGCATAA^{215}TGG. . .	MPVGLVLS	NC_006852
RbCoV-HKU14	208	5′. . .TAATCTA^{98}TGCTTGCGAGTGTAGATCTTTCAT^{111}AG. . .GTCATAA^{209}TGC. . .	MLASVDLS	NC_017083
HCoV-HKU1	205	5′. . .TTATCCA^{97}TGCTTGTGAGTGTGGTTT^{115}AA. . .GTCGCAA^{206}TGA. . .	MLVSVV	NC_006577
Betacoronavirus B				
SARS-CoV-Tor2	264	5′. . .GGCTGCA^{104}TGCCTAGTGCACCTACGCAGTATAAACAAT^{134}AA. . .GGTAAGA^{265}TGG. . .	MPSAPTQYKQ	NC_004718
Betacoronavirus C				
BtCoV-133/2005	258	5′. . .AGCTTCA^{133}TGCTCCACACTGGGCATAATT^{154}AA. . .CACACCA^{259}TGC. . .	MLHTGHN	NC_008315
TyBtCoV-HKU4	266	5′. . .AGCTTCA^{140}TGCTCAACACTGGGCATAATT^{161}AA. . .CATACTA^{267}TGC. . .	MLNTGHN	NC_009019
PiBtCoV-HKU5	260	5′. . .AAGCGCA^{141}TGTACACCACTGGGTATAATT^{162}AA. . .CACATCA^{261}TGT. . .	MYTTGYN	NC_009020
MERS-CoV	278	5′. . .GGACATA^{158}TGCTCAACACTGGGTATAATTCTAATT^{185}GA. . .CACATCA^{278}TGT. . .	MLNTGYNSN	NC_019843
Betacoronavirus D				
RoBtCoV-HKU9	228	(None). . .GTAGTGA^{229}TGG. . .		NC_009021
Gammacoronavirus				
IBV-Beaudette	528	5′. . .CCCTGGA^{131}TGGCACCTGGCCACCTGTCAGGTTTTTGTTATT^{164}AA. . .GACAACA^{529}TGG. . .	MAPGHLSGFCY	NC_001451
TCoV	528	5′. . .CCCTGGA^{131}TGGCACCTGGCCACCTGTCAGGTTTTTGTT^{161}AG. . .GACAACA^{529}TGG. . .	MAPGHLSGFC	NC_010800
CoV SW1	523	(None). . .GCAAACA^{524}TGT. . .		NC_010646
Deltacoronavirus				
NHCoV-HKU19	481	5′. . .GTTTTAA^{140}TGTCCGTACGTGTGCTTCACTAG. . .AAGAAGA^{482}TGG. . .	MSVRVLH	NC_016994
WiCoV-HKU20	218	(None). . .ACTAGTA^{219}TGG. . .		NC_016995
CMCoV-HKU21	477	5′. . .TGTTGGA^{29}TGCTAATTCGTTGGCATCAGTTAA. . .CTGACCA^{478}TGA. . .	MLIRWHQ	NC_016996
PorCoV-HKU15	538	5′ACA^{3}TGGGGACTAAAGATAAAAATTATAGCATTAGTCTATAA. . .TGTGAAA^{539}TGG. . .	MGTKDKNYSISL	NC_016990
SpCoV-HKU17	519	(None). . .TGAGAAA^{520}TGG. . .		NC_016992
MunCoV-HKU13	594	(None). . .TTTGGAA^{595}TGG. . .		NC_011550

MRCoV-HKU18	595	(None)...TTTGAGA$\underline{A}^{596}\underline{TG}$G...	NC_016993
ThCoV-HKU12	591	(None)...TCAGATA$^{592}\underline{TG}$G...	FJ376621
BuCoV-HKU11	606	(None)...ATAGATA$^{607}\underline{TG}$G...	FJ376619
WECoV-HKU16	510	(None)...TTTGATA$^{511}\underline{TG}$G...	NC_016991

[a] Data from GenBank (15 August 2013). TGEV-Purdue, porcine transmissible gastroenteritis virus Purdue strain (GenBank accession number DQ811788); FCoV, feline infectious peritonitis virus (accession number NC_002306); RhBtCoV-HKU2, *Rhinolophus* bat coronavirus HKU2 (accession number NC_009988); HCoV-NL63, human coronavirus NL63 (accession number NC_005831); HCoV-229E, human coronavirus 229E (accession number NC_002645); SCBtCoV-512, *Scotophylus* bat coronavirus (accession number NC_009657); PEDV, porcine epidemic diarrhea virus (accession number NC_003436); MiBtCoV-1A, bat coronavirus 1A (accession number NC_010437); MiBtCoV-1B, bat coronavirus 1B (accession number NC_010436); MiBtCoV-HKU8, bat coronavirus HKU8 (accession number NC_010438); RoBtCoV-HKU10, *Rousettus* bat coronavirus HKU10 (accession number NC_018871); BCoV-Mebus, bovine coronavirus strain Mebus (accession number U00735); HCoV-OC43, human coronavirus OC43 (accession number NC_005147); PHEV-VW572, porcine hemagglutinating encephalomyelitis virus (accession number NC_007732); ECoV, equine coronavirus (accession number NC_010327); MHV-A59, mouse hepatitis virus strain A59 (accession number NC_001846); MHV-JHM, mouse hepatitis virus strain JHM (accession number NC_006852); RbCoV-HKU14, rabbit coronavirus HKU14 (accession number NC_017083); HCoV-HKU1, human coronavirus HKU1 (accession number NC_006577); SARS-CoV-Tor2, SARS coronavirus isolateTor2 (accession number NC_004718); BtCoV-133/2005, bat coronavirus 133/2005 (accession number NC_008315); TyBtCoV-HKU4, *Tylonycteris* bat coronavirus HKU4 (accession number NC_009019); PiBTCoV-HKU5, *Pipistrellus* bat coronavirus HKU5 (accession number NC_009020); MERS-CoV, Middle East respiratory syndrome coronavirus or human betacoronavirus 2c EMC/2012 (accession number NC_019843); BtCoV-HKU9, bat coronavirus HKU9 (accession number NC_009021); IBV-Beaudette, avian infectious bronchitis virus strain Beaudette (accession number NC_001451); TCoV, turkey coronavirus (accession number NC_010800); CoV SW1, beluga whale coronavirus SW1 (accession number NC_010646); NHCoV-HKU19, night heron coronavirus HKU19 (accession number NC_016994); WiCoV-HKU20, wigeon coronavirus HKU20 (accession number NC_016995); CMCoV-HKU21, common moorhen coronavirus HKU21 (accession number NC_016996); PorCoV-HKU15, porcine coronavirus HKU15 strain HKU15-44 (accession number NC_16990); SpCoV-HKU17, sparrow coronavirus HKU17 (accession number NC_016992); MunCoV-HKU13, munia coronavirus HKU13-3514 (accession number NC_011550); MRCoV-HKU18, magpie-robin coronavirus HKU18 (accession number NC_016993); ThCoV-HKU12, thrush coronavirus HKU12-600 (accession number FJ376621); BuCoV-HKU11, bulbul coronavirus HKU11-934 (accession number FJ376619); WECoV-HKU16, white-eye coronavirus HKU16 (accession number NC_016991).

[b] Underlining identifies the putative translation start and stop codons for the uORFs. An optimal Kozak context is considered to be GCCA/GCC**AUGG** (see the text).

uORF *per se* was not necessary for virus replication in cell culture. In addition, the AUG-mutated uORF (but not the AUG-deleted uORF) correlated with a high virus titer in cell culture, and with a subcloned MHV 5′-proximal sequence that was translated *in vitro* in a rabbit reticulocyte translation system, the AUG-mutated uORF correlated with up to a 1.6-fold-higher translation yield. Therefore, the AUG-initiated uORF confers some attenuation of translation of the downstream (main) ORF1. Inspection of the group-classified reference strains of coronaviruses also revealed potential CUG-initiated uORFs in subgroup-specific distribution patterns. The potential CUG-initiated uORFs are described but were not studied further. These results together indicate that the MHV genomic AUG-initiated uORF, although it represses translation from ORF1, must play a beneficial role in virus survival in cell culture, as evidenced by uORF reselection following its disruption or removal. Further studies are needed to establish the nature of this benefit.

MATERIALS AND METHODS

Virus and cells. The A59 strain of MHV (GenBank accession number NC_001846) was used for reverse-genetics analyses (32). Delayed brain tumor (DBT) cells (33), mouse L2 cells (34), and baby hamster kidney cells expressing the MHV receptor (BHK-MHVR) (35, 36) were grown in Dulbecco's modified Eagle's medium (DMEM) supplemented with 10% defined fetal calf serum (FCS) (HyClone) and 20 μg/ml gentamicin (Invitrogen). Cells were maintained at 37°C with 5% CO_2 for all experiments. BHK-MHVR cells were maintained in selection medium containing 0.8 mg/ml Geneticin (G418 sulfate; Invitrogen) (32).

RNA structure prediction. The mfold program of Zuker (http://www.bioinfo.rpi.edu/zukerm/) (37, 38) was used for RNA structure predictions.

MHV reverse-genetics system. The reverse-genetics system for MHV-A59, infectious clone MHV-A59-1000 (icMHV), developed and kindly provided by Ralph Baric and colleagues (32), was used as previously described in detail for making 5′-proximal mutations in the MHV genome (39). Viral mutants were made by modifying fragment A (39) with the appropriate primers for the mutations described below. All procedures for mutant plasmid construction with icMHV DNA, plasmid DNA ligation, synthesis of full-length mutated recombinant viral RNA, transfection of cells with infectious recombinant RNA by electroporation, and characterization of mutant progeny by virus titration and growth kinetics were carried out as previously described (39). Plaque morphology was determined on L2 cells after 60 h of growth and after crystal violet staining, as described previously (39). Plaque sizes were identified as large (WT) if they were ≥2.5 mm, medium if they were 1.5 to 2.5 mm, or small if they were ≤1.5 mm in diameter. Plaque images were captured by laser scanning or by photography with a Nikon digital camera and prepared with Adobe Photoshop software.

Genome sequence analysis of virus progeny. Routinely, supernatant fluids from cells that first showed cytopathic effect (CPE) (either cells that had been transfected or cells that had been blind passaged) were collected, and the harvested virus was named virus passage zero (VP0). When 80 to 100% of new DBT cells infected with VP0 virus showed CPE, intracellular RNA was TRIzol (Invitrogen) extracted, and the viral genome was sequenced by reverse transcription-PCR (RT-PCR) for the 5′-proximal nt 22 to 1093. VP0 virus was then used to determine plaque morphology, and plaque-purified virus was used as the starting material for determining growth kinetics on DBT cells and sequence analyses.

For analysis of the 5′ nt 22 to 1093 of progeny virus genomes, extracted cellular RNA was reverse transcribed with Superscript II reverse transcriptase (Invitrogen), using primer MHV-1094(+) (5′-CGATCAACGTGCC AAGCCACAAGG-3′), which binds MHV genomic nt 1094 to 1117, and cDNA was PCR amplified with primers MHV-leader(−) (5′-TATAAGA GTGATTGGCGTCCG-3′), which binds nt 1 to 21 of the MHV antileader,

and MHV-1094(+). PCR products were gel purified (Qiaex II; Qiagen) prior to automated sequencing with primers MHV(261-284)(−) (5′-CCATGGATGCTTCCGAACGCATCG-3′) and MHV(605-623)(+) (5′-GTTACACAGGCAGACGCGC-3′).

Northern analysis. Northern analysis was done as previously described (40). Briefly, freshly confluent DBT cells in 25-cm^2 flasks (~4 × 10^6 cells) were infected with WT or mutant viruses at a multiplicity of infection (MOI) of 1.0 PFU/cell. At 20 h postinfection (hpi), intracellular RNA was TRIzol extracted, and 1/10 of the total RNA from one 25-cm^2 flask (~60 μg RNA total per 25-cm^2 flask) was resolved by electrophoresis in a 1.0% agarose-formaldehyde gel at 150 V for 4 h. RNA was transferred to a HyBond N$^+$ nylon membrane (Amersham Biosciences) by vacuum blotting for 3 h, followed by UV cross-linking. After prehybridization of the membrane with NorthernMax Prehybridization/Hybridization buffer (Ambion) at 55°C for 4 h, the blot was probed at 55°C overnight with 20 pmol (~4 × 10^5 cpm/pmol) of γ-^{32}P-5′-end-labeled 3′-UTR-specific oligonucleotide MHV(31094-31122)(+) (5′-CAGCAAGACATCCATTCTGATAGAGAGTG-3′), which binds MHV genomic nt 31094 to 31122. Probed blots were exposed to Kodak XAR-5 film at −80°C for imaging, and images were prepared by using Adobe Photoshop software.

Construction of plasmids for generating transcripts for *in vitro* translation. For *in vitro* translation analysis of a large portion of the nonstructural protein 1 (nsp1) gene containing the 5′ UTR with mutations, a WT construct was made, which fused the 5′-proximal 899 nt of the genome precisely with the 3′ UTR that has an attached 65-nt poly(A) tail. For this, plasmid A of the cloned MHV-A59 genome containing an upstream T7 promoter and all of the nsp1 coding region (32) was used to prepare the 5′-end fragment, and plasmid G (32) was used to prepare the 3′-end fragment. The final cloned sequence was made by overlapping the two PCR fragments at the junction sites, reamplifying with primers T7startMHV and EcoRI-65A-MHV(+), and cloning into the TOPO-XL vector (Invitrogen) between the two EcoRI sites. Plasmids with specific mutations were made by modifying the WT plasmid with the appropriate primers. Insert and junction sequences in all constructs were confirmed by DNA sequencing.

***In vitro* transcription.** To prepare RNA for *in vitro* translation, the DNA template was removed from the TOPO plasmid by EcoRI digestion and purified by gel electrophoresis. Capped transcripts were made with the T7 mMessage mMachine kit (Ambion), according to the manufacturer's protocol, which places the m7GpppG cap on ~80% of transcripts (Ambion).

***In vitro* translation.** For *in vitro* translation, 100 ng of transcript was translated for 1 h at 30°C in a 25-μl mixture containing 17.5 μl rabbit reticulocyte lysate (RRL) (Promega), 2 nM amino acid mixture minus methionine, 10 U RNasin RNase inhibitor (Promega), and 20 μCi of [^{35}S]methionine. Radiolabeled proteins were resolved by sodium dodecyl sulfate-polyacrylamide gel electrophoresis (SDS-PAGE) in gels of 12% polyacrylamide, and dried gels were exposed to Kodak XAR-5 film for imaging. Bands were removed, and radioactivity was quantitated by scintillation counting. Radioactive counts were normalized to the number of methionine bases in the WT. For a loading control, 500 ng of each sample was resolved by agarose gel electrophoresis, the gel was stained with ethidium bromide, and the image was captured by Fotodyne UV26 photography followed by band density quantitation using TINA version 2.0 (Raytest, Germany).

RESULTS

An AUG-initiated uORF is found in the genomes of a majority of coronavirus species. An analysis of sequenced coronavirus genomes available in GenBank showed that a uORF, similar to that depicted for MHV-A59 in Fig. 1B, is present usually in a suboptimal Kozak context in >75% of species, as represented by the 38 reference strains (Table 1). In the betacoronavirus subgroup, these include bovine coronavirus (BCoV), the highly studied MHV, severe acute respiratory syndrome coronavirus (SARS-CoV), and the recently identified Middle East respiratory syndrome coronavirus (MERS-CoV) (41). The uORF maps downstream of the (65- to 90-nt) common leader and potentially encodes a peptide of 3 to 13 amino acids (aa) in length (Table 1). An AUG-initiated uORF is not found in bat coronavirus HKU9-1, a currently categorized betacoronavirus D member; in beluga whale virus SW1, a gammacoronavirus; or in 7 of 10 recently characterized deltacoronaviruses (42) (Table 1). However, in these virus, inspection reveals the presence of one to eight potential CUG-initiated ORFs that could encode peptides of 2 to 89 aa (Table 2). Potential CUG-initiated uORFs are also present in most viruses with an AUG-initiated ORF as well, and interestingly, patterns of the potential CUG-initiated ORFs differ among the coronavirus subgroups (Table 2) (see Discussion).

It is notable that the AUG-initiated uORFs in the laboratory-studied betacoronaviruses MHV, BCoV, and SARS-CoV are found associated with a phylogenetically conserved stem-loop 4 (15, 31). Stem-loop 4 in BCoV (formerly called stem-loop III [15]) has been shown to be a *cis*-acting element in defective interfering (DI) RNA replication (15). However, as shown by Yang et al. (31), neither a functional uORF AUG codon nor a uORF-containing portion of stem-loop 4 is required for MHV replication. The significance of the association of the uORF with stem-loop 4 in betacoronaviruses is not known.

Translation of the uORF in MHV is observed when measured *in vitro* as a uORF-ORF1 fusion protein. In initial experiments to test for a translation product from the MHV uORF that contains a start codon within a suboptimal Kozak context, GUGUCC**AUG**C (where the optimal sequence is GCCG/ACC**AUG**G, in which underlining identifies the −3 and +4 nucleotide positions relative to A in the AUG start codon [in boldface] [43]), a WT construct was made, in which the 5′ 899 nt of the WT MHV-A59 genome (which includes the 5′ UTR and 93% of the N-proximal nsp1 coding region within ORF1) was attached to the genomic 3′ UTR and 65-nt poly(A) tail. From this construct, T7-generated transcripts were translated in RRL, and the [^{35}S]Met-radiolabeled products were resolved by SDS-PAGE. Since an 8-aa peptide from the uORF was not discernible on a polyacrylamide gel (data not shown), a fusion was made between the uORF and a partial nsp1 ORF and tested for translation in RRL. For this test, the three in-frame sequential stop codons for the uORF (U^{123}AG, U^{129}GA, and U^{138}AG) were converted to translatable codons (CAG, CGA, and CAG) to form a 5′-proximal sequence identical to that in virus mutant M3 (described below) (Fig. 2A). From this construct, T7 RNA polymerase-generated transcripts were made and translated in RRL in the presence of [^{35}S]Met. Polyacrylamide gel electrophoresis of the M3 translation products (Fig. 2C) revealed a fusion protein from the uORF (top band) and a product starting from nt 210 (and possibly also nt 219) (bottom band). These results indicate that although there is probable leaky scanning through the uORF leading to synthesis of the shorter of the two products, the uORF does function as a translation template that makes the fusion protein *in vitro* and therefore is likely to be translated *in vivo* as an independent uORF.

To examine the viability of a recombinant virus containing these mutations, mutant M3 virus was made and tested. M3 virus grew within 48 h posttransfection (hpt) with recombinant RNA and replicated in cell culture to titers similar to those of the WT (Fig. 2D), and an RT-PCR test of the M3 genomic RNA sequence within cells at virus passage 3 revealed that it had maintained the

TABLE 2 Potential coronavirus CUG-initiated uORF sizes in 38 GenBank reference strains

Virus[a]	5′ UTR (nt)	Potential CUG-initiated uORF and ORF1 start codons within the Kozak context[b]	uORF peptide length (aa)	GenBank accession no. of reference sequence
Alphacoronavirus				
TGEV-Purdue	314	(None). . .AGGAGAA^{315}TGA. . .		DQ811788
FCoV	311	5′. . .CCGTCCC^{209}TGT. . .T^{312}GA. . .	34	NC_002306
		TATTAGC^{236}TGC. . .T^{257}AG. . .AGGAGAA^{312}TGA. . .	7	
RhBtCoV-HKU2	296	5′. . .ATCTATC^{21}TGT. . .T^{45}AG. . .	8	NC_009988
		CCCACGC^{232}TGT. . .T^{259}AG. . .	9	
		GCTGTTC^{251}GTT. . .T^{276}GA. . .	13	
		CGATAAC^{288}TGT. . .GCACAA^{297}TGT. . . (joins ORF 1)	3	
HCoV-NL63	286	5′. . .CTAGTGC^{89}TGT. . .TTTGTTA^{101}TGG. . . (joins AUG-initiated uORF)	4	NC_005831
		TGTAAAC^{143}TGG. . .T^{197}AG. . .	18[c]	
		TAAGCAC^{180}TGG. . .T^{216}AA. . .	12[c]	
		CCGTCAC^{233}TGC. . .T^{275}AA. . .GCTAACCA^{287}TGT. . .	14	
HCoV-229E	292	5′. . .TTGATGC^{105}TGG. . .T^{114}AG. . .	3[c]	NC_002645
		CAAGTGC^{161}TGT. . .T^{177}AA. . .	5	
		AAAGTTC^{262}TGT. . .T^{328}GA. . .TTCCTAA^{293}TGG. . . (overlaps ORF1 start)	23	
ScBtCoV-512	293	5′. . .GTCGTGC^{166}TGC. . .T^{289}AG. . .	41	NC_009657
		GAAAGTC^{258}TGT. . .T^{273}GA. . .TTAGCTA^{294}TGG. . .	5	
PEDV	296	5′. . .GCTGTGC^{169}TGT. . .T^{271}AG. . .	34	NC_003436
		TAGTTCC^{183}TGG. . .T^{213}AG. . .CCGGCTA^{297}TGG. . .	10	
MiBtCoV-1A	271	5′. . .AGGTGGC^{195}TGC. . .T^{264}AGCAGGTA^{272}TGT. . .	23	NC_010437
MiBtCoV-1B	272	5′. . .TTCCGTC^{166}TGT. . .T^{233}AG. . .	19	NC_010436
		AAGTGGC^{196}TGC. . .T^{265}AGCAGGTA^{273}TGC. . .	23	
MiBtCoV-HKU8	268	5′. . .TTTAGAC^{48}TGT. . .T^{69}AA. . .	7	NC_010438
		CTCGCAC^{166}TGT. . .T^{205}AG. . .	13	
		AAACCAC^{189}TGT. . .T^{249}GA. . .GTCGCTA^{269}TGG. . .	20	
RoBtCoV-HKU10	301	5′. . .TTCTATC^{28}TGC. . .T^{52}AG. . .	8	NC_018871
		GTGGCTC^{190}TGA. . .T^{250}GA. . .	20[c]	
		TCTTGTC^{281}TGA. . .T^{308}AG. . .TGCCCAA^{302}TGG. . . (overlaps ORF1 start)	9	
Betacoroanvirus A				
BCoV-Mebus	210	5′. . .GCTTCAC^{37}TGA. . .T^{113}AG. . .	4	U00735
		TCATTTC^{145}TGC. . .T^{184}AG. . .GTCACAA^{211}TGT. . .	13	
HCoV-OC43	210	5′. . .GCTTCAC^{37}TGA. . .T^{49}AG. . .	4	NC_005147
		TCATTTC^{145}TGC. . .T^{184}AG. . .GTCACAA^{211}TGT. . .	13	
PHEV-VW572	210	5′. . .GCTTCAC^{37}TGA. . .T^{49}AG. . .	4	NC_007732
		TCATTTC^{145}TGC. . .T^{184}AG. . .GTCACAA^{211}TGT. . .	13	
ECoV	208	5′. . .GCTTCAC^{37}TGA. . .T^{49}AG. . .	4	NC_010327
		TTTCTAC^{147}TGT. . .T^{183}AG. . .GTCACAA^{209}TGG. . .	12	
MHV-A59	209	5′. . .ATAGTGC^{128}TGA. . .T^{146}GA. . .	6[c]	NC_001846
		CGUUCUC^{159}TGC. . .A^{210}TGG. . . (joins ORF1)	17–ORF1	
MHV-JHM	214	5′. . .CACTTGC^{94}TGC. . .T^{151}GA. . .	19	NC_006852
		CGTTCTC^{164}TGC. . .A^{215}TGG. . . (joins ORF1)	17–ORF1	
RbCoV-HKU14	208	5′. . .GATTC^{5}TGA. . .T^{59}AA. . .GTCATAA^{208}TGC. . .	18[c]	NC_017083
HCoV-HKU1	205	5′. . .ATCTCTC^{158}TGC. . .T^{197}AG. . .GTCGCAA^{206}TGA. . .	13	NC_006577
Betacoronavirus B				
SARS-CoV-Tor2	264	5′. . .GTAGATC^{56}TGT. . .T^{86}AG. . .	10	NC_004718
		TAAAATC^{81}TGT. . .T^{153}GA. . .	24	
		GTGTAGC^{81}TGT. . .A^{104}TG. . . (joins AUG-initiated uORF)	5	
		GCTCGGC^{100}TGC. . .T^{109}AG. . .	3	
		ATTTTAC^{146}TGT. . .T^{167}AA. . .	7	
		CCTCTTC^{182}TGC. . .T^{233}AG. . .	17	
		TGCAGAC^{189}TGT^{261}AA. . .GGTAAGA^{265}TGG. . .	24	
Betacoronavirus C				
BtCoV-133/2005	258	5′. . .GCCTTGC^{88}TGT. . .T^{111}AG. . .	11	NC_008315
		TGTGGTC^{101}TGC. . .T^{167}AA. . .	22	
		TTCATTC^{184}TGA. . .T^{301}AA. . .CACACCA^{259}TGC. . . (overlaps ORF1 start)	39[c]	
TyBtCoV-HKU4	266	5′. . .GCCTTGC^{85}TGT. . .T^{118}AG. . .	11	NC_009019
		TGTGGTC^{108}TGC. . .T^{174}AA. . .	22	
		TTCATTC^{191}TGA. . .T^{281}AG. . .	30[c]	
		AATACCC^{231}TGT. . .CATACTA^{267}TGC. . . (joins ORF1)	12	
PiBtCoV-HKU5	260	5′. . .TGCGTGC^{95}TGC. . .T^{119}AG. . .	8	NC_009020
		ACCTTTC^{108}TGC. . .A^{141}TG. . .	11	
		ACACCAC^{151}TGG. . .T^{172}AA. . .	7	
		TTAAAAC^{167}TGA. . .T^{307}AG. . .CACATCA^{261}TGT. . . (overlaps ORF1 start)	47[c]	
MERS-CoV	288	5′. . .ACTTGTC^{110}TGG. . .T^{188}AA. . .CACATCA^{289}TGT. . .	6	NC_019843
Betacoronavirus D				
RoBtCoV-HKU9	228	5′. . .GTCTTGC^{16}TGT. . .T^{157}AA. . .	47	NC_009021
		GTCGTCC^{192}TGT. . .T^{243}GA. . .GTAGTGA^{229}TGG. . . (overlaps ORF1 start)	17	

(Continued on following page)

TABLE 2 (Continued)

Virus[a]	5′ UTR (nt)	Potential CUG-initiated uORF and ORF1 start codons within the Kozak context[b]	uORF peptide length (aa)	GenBank accession no. of reference sequence
Gammacoronavirus				
IBV-Beaudette	528	5′. . .CTACAGC^{86}TGG. . .T^{119}AG. . .	15	NC_001451
		TGGCACC^{136}TGG. . .T^{396}GA. . .	86	
		ATACATC^{221}TGT. . .T^{299}AG. . .	26	
		GAACCTC^{289}TGG. . .T^{448}AG. . .	53	
		CAGGTTC^{486}TGG. . .T^{522}GACAACA^{529}TGG. . .	12[c]	
TCoV	528	5′. . .CTACAGC^{86}TGG. . .T^{161}AG. . .	15	NC_010800
		AGTGCCC^{117}TGG. . .T^{169}AA. . .	14[c]	
		TGGCACC^{138}TGG. . .T^{396}GA. . .	86	
		CAGGTTC^{486}TGG. . .T^{522}GACAACA^{529}TGG. . .	12[c]	
CoV SW1	523	5′. . .TGTTTCC^{98}TGA. . .T^{272}AA. . .	58	NC_010646
		TGGCAGC^{126}TGG. . .T^{360}AG. . .	78	
		CGGCTTC^{151}TGG. . .T^{406}AA. . .	24	
		TTCTACC^{244}TGG. . .T^{406}AA. . .GCAAACA^{524}TGT. . .	54	
Deltacoronavirus				
NHCoV-HKU19	481	5′. . .ACCATTC^{115}TGA. . .T^{271}AG. . .	52[c]	NC_016994
		GCCCCTC^{189}TGT. . .T^{303}AG. . .	38	
		CCGAGCC^{299}TGG. . .T^{368}GA. . .	23[c]	
		CTCAAGC^{393}TGA. . .T^{441}AG. . .AAGAAGA^{482}TGG. . .	16[c]	
WiCoV-HKU20	218	5′. . .TCAGGAC^{129}TGC. . .T^{144}AG. . .	5	NC_016995
		GGCACTC^{200}TGG. . .T^{215}AG. . .ACTAGTA^{219}TGG. . .	5[c]	
CMCoV-HKU21	477	5′. . .TACGTGC^{94}TGC. . .T^{133}AA. . .	13	NC_016996
		ATTTTGC^{122}TGT. . .T^{203}AG. . .	27	
		CGTATTC^{404}TGT. . .T^{416}AA. . .	4	
		CCTATTC^{447}TGC. . .T^{465}AA. . .ACCA^{478}TGA. . .	6	
PorCoV-HKU15	538	5′. . .GTGCGTC^{93}TGC. . .T^{207}AG. . .	38	NC_016990
		GTTCCTC^{254}TGA. . .T^{284}GA. . .	10	
		ACAGCAC^{284}TGA. . .T^{430}AG. . .	30[c]	
		ACCGGTC^{314}TGC. . .T^{395}GA. . .	27	
		AGTGATC^{451}TGA. . .T^{481}GA. . .	10[c]	
		TCTGATC^{456}TGG. . .T^{525}GA. . .TGTGAAA^{539}TGG. . .	23[c]	
SpCoV-HKU17	519	5′. . .GGGGCGC^{106}TGT. . .T^{328}AG. . .	74	NC_016992
		GATTACC^{133}TGG. . .T^{254}AG. . .	40	
		GTTCCTC^{234}TGG. . .T^{264}GA. . .	10	
		ACAGCAC^{263}TGA. . .T^{353}AG. . .	30[c]	
		ACCGGTC^{294}TGC. . .T^{417}AG. . .	41	
		TCTGATC^{436}TGG. . .T^{505}GA. . .TGAGAAA^{520}TGG. . .	23[c]	
MunCoV-HKU13	594	5′. . .CTTTGGC^{116}TGA. . .T^{347}AG. . .	77	NC_011550
		TGGTCAC^{132}TGC. . .T^{207}AG. . .	25	
		AAAGGCC^{229}TGG. . .T^{268}AG. . .	13[c]	
		AGTGATC^{506}TGA. . .T^{545}AG. . .	13[c]	
		TCTGATC^{511}TGG. . .T^{580}GA. . .	23[c]	
		GCAGCTC^{573}TGT. . .T^{585}AG. . .TTTGGAA^{595}TGG. . .	4	
MRCoV-HKU18	595	5′. . .AACGGCC^{151}TGG. . .T^{190}AG. . .	13[c]	NC_016993
		GGCTCGC^{161}TGG. . .T^{350}AG. . .	63	
		CACGGCC^{229}TGG. . .T^{268}AG. . .	13[c]	
		TCTTCTC^{298}TGT. . .T^{331}AG. . .	11	
		GTTAAGC^{360}TGT. . .T^{429}AG. . .	23	
		ACCGGTC^{370}TGC. . .T^{493}AG. . .	41	
		AGTGATC^{507}TGA. . .T^{546}AG. . .	13[c]	
		TCTGATC^{512}TGG. . .T^{581}GA. . .TTTGAGA^{596}TGG. . .	23[c]	
ThCoV-HKU12	591	5′. . .ATTTTGC^{35}TGC. . .T^{302}AA. . .	89	FJ376621
		TACTACC^{217}TGT. . .T^{235}AG. . .	6	
		ATTCCTC^{316}TGA. . .T^{454}AA. . .	46	
		AGTGACC^{503}TGA. . .T^{542}AG. . .	13[c]	
		CCTATTC^{562}TGC. . .T^{580}AA. . .	6	
		AGCTGCC^{572}TGA. . .T^{598}GA. . .TCAGATA^{592}TGG. . . (overlaps ORF1 start)	9	
BuCoV-HKU-11	506	5′. . .GTTGTGC^{94}TGG. . .T^{115}AG. . .	7[c]	FJ376619
		CAGTGCC^{105}TGC. . .T^{141}AA. . .	12	
		TTTCGGC^{168}TGT. . .T^{255}AG. . .	29	
		GATTGTC^{179}TGT. . .T^{212}GA. . .	11	
		TACTTGC^{339}TGA. . .T^{360}AG. . .	7	
		ACCGGTC^{380}TGC. . .T^{497}AG. . .	39	
		CCTATTC^{577}TGC. . .T^{595}AG. . .	6	
		AGCTGCC^{587}TGA. . .T^{602}AGATA^{607}TGG. . .	5	
WECoV-HKU16	510	5′. . .ACAAAGC^{8}TGA. . .T^{44}AG. . .	12[c]	NC_016991
		CTTAGGC^{95}TGG. . .T^{128}AG. . .	12[c]	
		GAACTAC^{135}TGG. . .T^{255}AA. . .	40	
		ACCGCTC^{294}TGC. . .T^{408}AG. . .	38	
		TCTAAGC^{377}TGT. . .T^{461}AG. . .	28	
		GGCTCGC^{491}TGG. . .T^{584}AA. . .TTTGATA^{511}TGG. . . (overlaps ORF1 start)	31	

[a] Data from GenBank (15 August 2013).

[b] An optimal Kozak context is considered to be GCCA/GCC**AUG**G (see the text).

[c] Has a purine in the −4 and +1 positions at the ORF for this peptide, denoting a potentially "good to excellent" Kozak context for translation initiation.

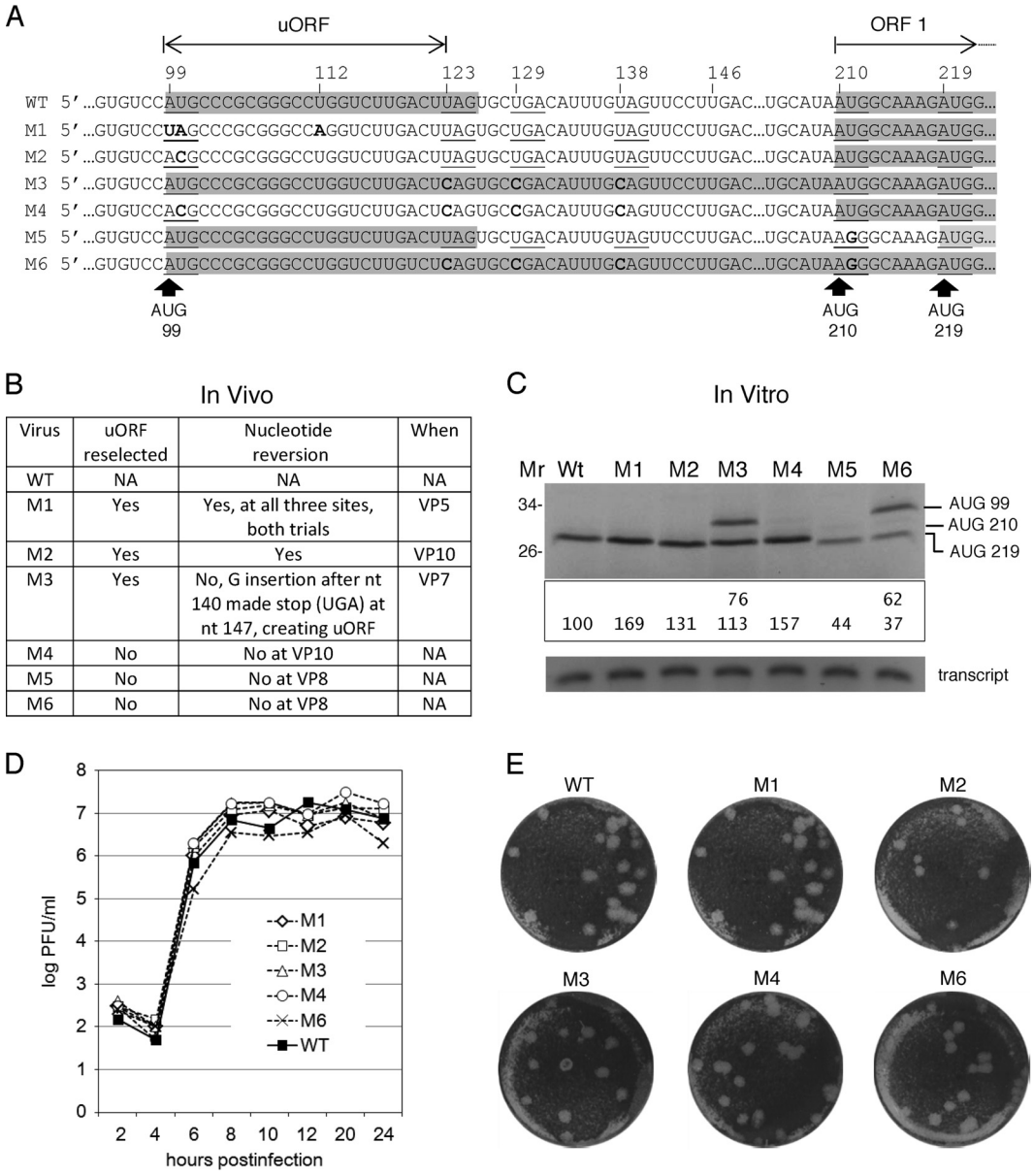

FIG 2 Disruptive point mutations in the uORF and subsequent reselection of the uORF. (A) Description of mutations in M1 through M6. ORFs are identified by shading. Mutated nucleotides are identified by boldface type. Bold arrowheads identify positions of WT start codons. The naturally occurring translation start and stop codons are underlined. Nucleotides are numbered beginning with the genome 5′ end. (B) Summary of WT and mutant recombinant virus behavior for M1 through M6. VP, virus passage; NA, not applicable. (C) Electrophoresis of radiolabeled proteins from *in vitro* (RRL) translation reactions in one representative experiment. (Top) SDS-PAGE of *in vitro*-synthesized nsp1 protein or the uORF-nsp1 fusion protein from 100 ng of RNA transcript. Quantitation was determined by scintillation counting of excised bands. (Middle) Percentage of methionine-normalized counts relative to those in the WT band. (Bottom) Separate ethidium bromide-stained agarose gel showing electrophoretically separated RNA from 500 ng loaded per lane. (D) A single growth kinetics analysis where the MOI was 1.0 for the WT and M1 through M6. (E) Plaques of WT, M1, M2, M3, M4, and M6 viruses.

fusion genotype (not shown). However, it was not determined whether the replicating virus used a fused translation product or used the ORF1 product initiating from the site at nt 210. The surprise from this experiment was that the uORF-ORF1 fusion virus was viable, and its replication was robust, judging from both plaque size and growth kinetics. This mutant was also surprisingly stable since the fused genotype remained for six passages (described below).

None of four virus mutants with uORF-disrupting mutations showed debilitated growth in cell culture, yet a uORF in three mutants was reselected within 10 virus passages. To test whether translation of the uORF in the virus genome is needed for virus replication in cell culture, four mutants were studied. In the first mutant, M1, the uORF was blocked by changing its AUG start codon to a UAG stop codon, and a U112A mutation was also made to maintain a stem-loop 4 structure previously shown to be a *cis*-acting requirement for bovine coronavirus DI RNA replication (15). In two separate experiment trials, starting in each case with freshly synthesized recombinant RNA from ligated mutated plasmid DNA fragments, recombinant virus was recovered from transfection, and when measured at the first viral passage, the

progeny had WT-like plaques and WT-similar growth kinetics (Fig. 2D and E) but the fully mutated sequence. By passage 5, it was found by RT-PCR sequencing analysis with RNA from infected cells that the three mutated sites had reverted to the WT (Fig. 2B). In addition, plasmid constructs of M1 were used to generate transcripts for *in vitro* translation in the same manner as described above for the WT and M3, and transcripts were translated in RRL. From M1, as from the WT, only a single band of protein initiating from the ORF1 start site at nt 210 was observed (Fig. 2C, top). From experiments with M1, therefore, we conclude that a separate uORF entity is not necessary for virus replication in cell culture but is nevertheless rapidly reselected within four viral passages. The uORF therefore may provide a survival advantage for the virus.

To determine if the uORF AUG would be reselected from a second type of ORF-disrupting mutation, M2 was made, in which the genome sequence was the WT sequence except that ACG, a weak noncanonical start codon (44), replaced the AUG uORF start codon. In M2, in which ORF1 starting at nt 210 is the first AUG-initiating codon to be approached by a scanning ribosome (Fig. 2A), viable virus was recovered within 48 hpt, and both progeny plaques and growth kinetics were similar to those of the WT (Fig. 2D and E). Reversion to a WT uAUG codon in M2 was not observed until virus passage 10 (Fig. 2B). Conceivably, the uCUG at nt 111 in M2, encoding a potential peptide of 4 aa, could have initiated uORF translation and therefore functionally replaced the WT AUG-initiated uORF. However, this appears unlikely since there was extremely little product made of the size expected for the uCUG-ORF1 fusion protein initiating at nt 111 in M4 (described below). By gel electrophoresis, the product size from the *in vitro* translation of M2 was the same as that from the WT and M1 (Fig. 2C).

To test for reselection, a third type of mutant, M3, containing the uORF fused in frame with ORF1 as described above, was studied. Since a separate uORF could be reselected by formation of not only a new AUG start codon but also a new stop codon within the contiguous uORF-ORF1 fused region (Fig. 2A), reselection by either of these mechanisms was sought by further passaging of M3 progeny. For this, the 5′-UTR sequence was determined in each of eight serial passages of progeny virus. Interestingly, at passage 7, a G insertion was found just after nt 140, which created a frameshift and a consequential UGA stop codon beginning at nt 147 that extended the original 8-codon uORF to 16 codons.

To test for reselection of the uORF in a fourth mutant type, M4 was made, in which the mutation in M2 (a uORF AUG→ACG conversion) was combined with the mutations in M3 (conversion of the three in-frame stop codons to nonstop codons) (Fig. 2A). Reselection of a uORF in this case would require a reversion of ACG to AUG or the formation of a new AUG along with a reversion of one of the coding sequences CAG, CGA, and CAG to a stop codon or the formation of a new stop codon elsewhere. M4 was immediately viable following RNA transfection, and the plaque size and virus growth kinetics were similar to those of the WT (Fig. 2D and E). After 10 passages, there was no re-formation of a uORF (Fig. 2B). Regarding the question of whether or not the CUG-initiated short uORF in M2 is translated, synthesis of a second large polypeptide during M4 translation *in vitro* would have indicated that it is. As is evident from the M4 product shown in Fig. 2C, only a very small amount of *in vitro*-generated fusion protein was made, indicating that initiation from uCUG was probably minimal (note the faint band immediately above the major band in the M4 lane). It may be, however, that uCUG-initiated translation is more robust in virus-infected cells.

Thus, under the conditions of these experiments with M1, M2, M3, and M4, it appears that a uORF is not necessary for virus replication in cell culture, but it may provide a survival advantage or degree of fitness for MHV replication that leads to its reselection.

Point mutations that disrupt the uORF cause an increased rate of translation from the (main) ORF1 start codon *in vitro*. Our analyses of translation initiation downstream of the uORF have assumed that it begins at nt 210. However, just 9 nt downstream, beginning at nt 219, an alternate AUG is found in a good Kozak context, which could function as the site for translation initiation (Fig. 2A). To establish whether the AUG at nt 219 can initiate translation of ORF1, the AUG at nt 210 in WT and M3 mutant viruses was converted to a nonstart AGG codon to create M5 and M6, respectively (Fig. 2A), and *in vitro* translation products of these mutants were compared with those of the WT and M1 through M4 (Fig. 2C). As can be observed, the putative nonfused products of M5 and M6 are slightly smaller and in smaller amounts than the product beginning at the AUG at nt 210, indicating that there is a translation product initiating at nt 219 and that it is less abundant. Interestingly, viruses produced from transfected M5 and M6 recombinant genomes were viable and revealed no reselection of a uORF after eight virus passages (Fig. 2B). M6 made WT-like plaques and had WT-like growth kinetics (Fig. 2D; M5 was unavailable for growth kinetic analysis). It was therefore concluded that the AUG at nt 210 was the bona fide start codon used in M1 through M4 and reflected the natural ORF1 start codon.

To determine whether the uORF has an influence on the rate of translation from ORF1, the M1 through M6 constructs containing the partial nsp1 ORF were used to determine translatability in RRL relative to the WT (Fig. 2C). To quantitate the relative amounts of protein produced, [^{35}S]Met was used in the translation reaction mixture, and protein bands identified by exposure of the gel to X-ray film were isolated and quantified by scintillation counting. As shown in Fig. 2C (top), the product from each construct excepting M5 and M6 appeared more abundant than the WT. In the case of M3 and M6, two products were made, probably due to initiation at the uORF to yield the fusion product and separate initiation at the ORF1 start site to yield the shorter product. Radioactivity quantitation demonstrated that the level of translation was higher in each mutant than in the WT (100%), ranging from 169% in M1 to 113% in M3 (Fig. 2C, middle panel, bottom band). Five hundred nanograms of each transcript was separately analyzed by electrophoresis in a nondenaturing agarose gel and stained with ethidium bromide as a loading control (Fig. 2C, bottom). Thus, the uORF has the effect of repressing translation from ORF1 *in vitro* in RRL.

Deletion mutations of 20, 30, and 51 nt, all within stem-loop 4 and each removing the uAUG and a large portion of the uORF, replicated, but only in the first two mutants did 10 passages of virus progeny reveal an alternate AUG-initiated uORF. To determine whether uORF removal would affect replication, constructs with deletions of four different sequence lengths that included the uAUG (Fig. 3A) were tested. Consistent with the findings of Yang et al. (31) and also extending them, our results demonstrate that deletions of 20, 30, and 51 nt of stem-loop 4,

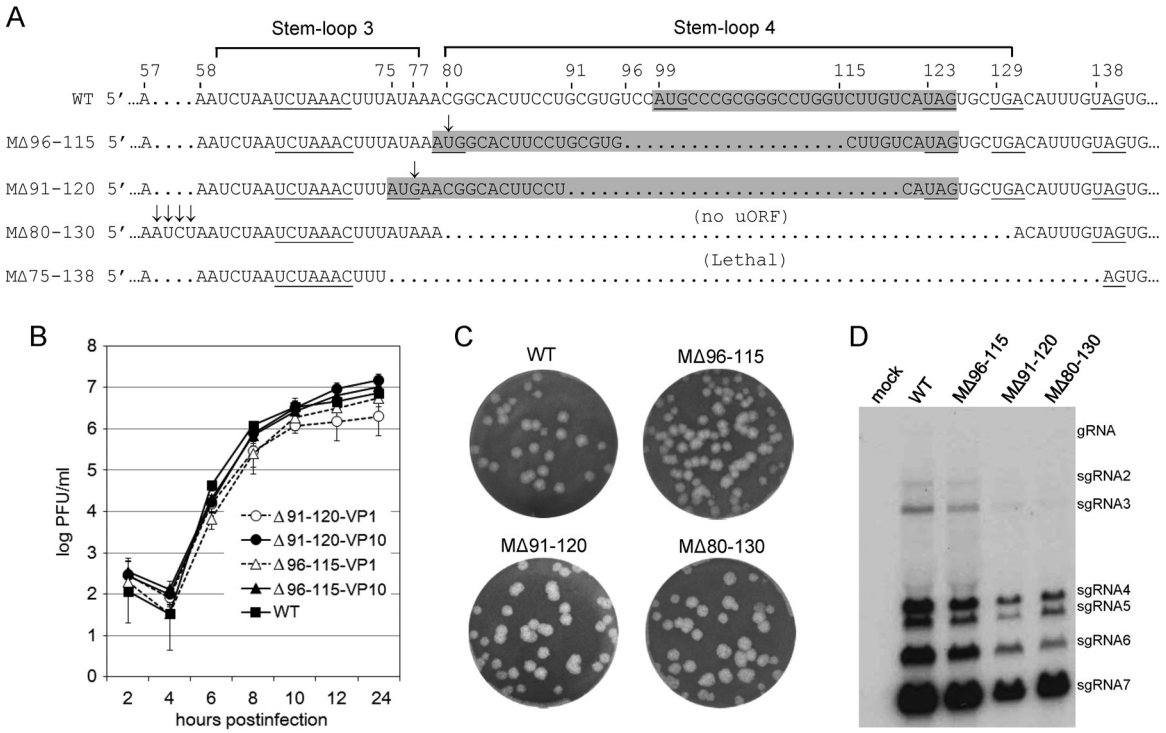

FIG 3 Deletion mutations and subsequent reselection of uORFs in progeny virus. (A) WT sequence positions of stem-loops 3 and 4 as noted in Fig. 1. The uORF is shown by shading. The heptameric RdRp template-switching signal, UCUAAAC, is underlined. In mutant virus MΔ96–115, the C80U transition causing a new uAUG in virus passage 10 is identified with a ↓. In mutant virus MΔ91–120, the A77G transition causing a new uAUG in virus passage 10 is identified with a ↓. In MΔ80–130, a 4-nt insertion, AUCU, occurs between nt 57 and 58 by virus passage 10, but no new uORF is formed by this insertion. Note that this insertion creates a new UCUAA element, a spontaneous phenomenon previously described for the MHV genome near this site. With mutant MΔ75–138, no progeny virus was recovered following recombinant RNA transfection. (B) Growth kinetics analyses where the MOI was 1.0 for the WT and mutants at virus passages 1 and 10. (C) Virus plaques at 48 hpi for WT and mutant viruses at virus passage 1. (D) Northern analysis for each replicating virus using a hybridization probe that identifies a 3′-end sequence. The same number of cells was used to prepare RNA for each lane.

which includes the AUG of the uORF, and 17 nt (70%), 22 nt (91%), and 24 nt (100%) of the uORF, respectively, can be made without a loss of virus viability. Only the fourth mutant, with a deletion of 64 nt that extended beyond both ends of stem-loop 4 (as depicted in Fig. 1B), was lethal, as was the same deletion in the study by Yang et al. (31) (Fig. 3A). By mfold analysis, stem-loop 4 becomes shortened but not otherwise distorted in mutants with deletions of 20 nt (MΔ96–115) and 30 nt (MΔ91–120) (Fig. 1B and 3A and data not shown). For the three viable deletion mutants, WT-like plaques at virus passage 1 were found for each mutant (Fig. 3C), but only mutants with deletions of 20 nt (MΔ96–115) and 30 nt (MΔ91–120) had a reselected uORF after 10 passages as a result of upstream C80U and A77G transitions, respectively (Fig. 3A), and an accompanying return to WT-like growth kinetics (Fig. 3B). Mutants with the two largest deletions, 30 nt (MΔ91–120) and 51 nt (MΔ80–130), showed dramatically reduced RNA production, as observed by Northern analysis (Fig. 3D). Thus, our experiments confirmed the observations of Yang et al. that showed that large portions of stem-loop 4 can be deleted without killing the virus (31) but also extended them to include the observations that (i) a precise deletion of stem-loop 4, i.e., nt 80 through 130, as defined in Fig. 1B and as modeled by Chen and Olsthoorn (45), is also not lethal or restrictive of sgmRNA synthesis and (ii) passaging of virus with deletions of nt 96 through 115 and nt 91 through 120 led to reselection of a uORF. Interestingly, in our viable deletion mutant of nt 80 through 130, an insertion of 4 nt, AUCU, was found between nt 57 and 58 at virus passage 10, which led to a new UCUAA element upstream of the leader fusion site for leader acquisition. A similar insertion was found by Yang et al. (31) and was also found to occur spontaneously in a similar position in WT MHV during passaging in cell culture (46). It is also part of a UCUAA sequence at this position in the MHV-JHM strain (GenBank accession number X00990) that is not present in the MHV-A59 strain (47).

Thus, as with the uORF-disrupting point mutations, disruption of the uORF by deletions was not necessarily lethal for the virus, but the uORF nevertheless, as indicated by its reappearance, apparently plays a beneficial role in the virus in cell culture. The surprise in these experiments was that the entire stem-loop 4 (nt 80 through 130) could be deleted without killing the virus. Therefore, while stem-loop 4 was identified as a *cis*-acting replication element for BCoV DI RNA, it was not found to be similarly required for the replication of the intact MHV genome (15, 31; this study).

DISCUSSION

Translation of the coronavirus genome and sgmRNAs has been presumed to follow cap-dependent 5′-end ribosomal entry and ribosomal scanning. This is based on the presence of a methylated cap on genomic RNAs and sgmRNAs (48), on the presence of virus-encoded enzymes involved in capping (19–24), and on evidence that cap-inhibiting drugs impair virus replication (49). The

role of a nearly universally found intra-5′-UTR AUG-initiated uORF in the coronavirus genome as a potential regulator of 5′-end scanning-dependent translation, however, is not known. Here, we have used MHV as a model coronavirus in cell culture to test the hypothesis that the single AUG-initiated uORF is translated and thereby functions to regulate ORF1 (the main ORF) translation and, consequently, virus replication. The data show that while disruption of the uAUG codon enhances translation of ORF1 *in vitro*, the mutation has no discernible effect on virus replication, as measured in cell culture during a 24-h infection period (Fig. 2). Furthermore, only moderate effects on virus replication were observed when partial or total deletions of the uORF were made, which might have been due to structural changes in the *cis*-acting stem-loop 4 or other structures and not translation of the uORF *per se* (Fig. 3) (15, 31). The data also show that a uORF was reselected within 10 virus passages for each of three methods used to disrupt the uORF: (i) mutations within the AUG start codon, (ii) fusion of the uORF with the main ORF (ORF1), and (iii) deletion of part or all of the uORF (Fig. 2 and 3). Restoration of a uORF by reselection brought back a near-WT-like phenotype in virus that had been debilitated by partial or complete deletion of the uORF. Therefore, it appears that one function of the AUG-initiated uORF is to attenuate ORF1 translation such that it provides a currently unidentified advantage for virus survival.

A genomic AUG-initiated uORF is not found in some coronaviruses (Table 1). These include bat coronavirus HKU9, a group D betacoronavirus; beluga whale coronavirus SW1, a gammacoronavirus; and wigeon coronavirus HKU20, sparrow coronavirus HKU17, munia coronavirus HKU13-3514, magpie-robin coronavirus HKU18, thrush coronavirus HKU12-600, bulbul coronavirus HKU11-934, and white-eye coronavirus HKU16, all members of the deltacoronavirus subgroup (42). Since the noncanonical CUG initiator codon is known to function to initiate translation in some cases, including uORFs (2, 50–54), potential CUG-initiated uORFs were sought by inspection of coronavirus genomes. Interestingly, one or more potential CUG-initiated uORFs can be found in almost all coronaviruses (Table 2), but only in the deltacoronaviruses are the CUG codons in a good enough Kozak context (−3A/G and +4A/G) (55) for likely use, suggesting that some deltacoronaviruses may use a CUG-initiated uORF in place of an AUG-initiated uORF. The potential in-frame uCUG initiator codon in MHV-A59 in a good Kozak context (AUAGUG**C**^{128}**UG**A) (Table 2) appears to make only a very minor amount of protein via *in vitro* translation (discussed above as a barely perceptible band in Fig. 2C, lane M4); however, this amount could be larger *in vivo*.

One role that the uORF might play in the coronavirus genome is that of repressing ORF1 translation relative to the amount of translation products needed from the sgmRNAs, which (mostly) carry no uORF. Since during coronavirus replication, the structural proteins are needed in far greater abundance than the nonstructural replicase proteins, repression of translation from ORF1 may be a mechanism that keeps the relative amounts optimal. In a sense, this is a conceptual extension of the frameshifting regulatory paradigm within ORF1 that maintains an optimal ratio of ORF1a to ORF1b proteins (56, 57). Another possible role might be that the uORF contributes to long-term virus survival in cells during persistent infection. This is suggested by the spontaneous appearances of uORFs during development of persistent infections. In one example, a G5A spontaneous mutation developed during persistent infection with bovine coronavirus that formed a novel 5′-proximal short AUG-initiated intraleader uORF (58). Because this uORF is in the common leader, it is also present in the 5′ UTR of sgmRNAs, and its repressive effects would be expected for all viral mRNAs. *In vitro* translation analysis demonstrated that the presence of the novel uORF correlated with repression of sgmRNA7 translation (58). In a second example, an A77G mutation in MHV was found only in the genomic 5′ UTR arising during persistent infection in cultured cells that led to a 24-nt 5′-ward extension of the natural AUG-initiated uORF (59). A mechanistic connection between this mutation and virus persistence, however, is more difficult to envision, since the A77G mutation caused an ~2.5-fold enhancement of translation, as determined by *in vitro* measurement, and an ~3.5-fold increase in p28 (nsp1) abundance, as determined by *in vivo* measurement (59). Curiously, this was the same spontaneous mutation that occurred in MΔ91-120 (Fig. 3A) that restored a WT-like phenotype to the deletion mutant (Fig. 3C).

More studies are needed to determine how the subtle effects of the uORF described here might be involved in the more dramatic translation regulatory events associated with acute coronavirus infection. For MHV, these include the property of robust viral protein synthesis at a time when there is global inhibition of host cell translation, presumably as a function of α subunit of eukaryotic initiation factor 2 (eIF2α) phosphorylation (60–63). eIF2α phosphorylation blocks formation of the 40S rRNA-GTP-eIF2α ternary complex required for cap-dependent initiation of translation (64). Interestingly, translation of MHV mRNA appears enhanced under these conditions, apparently as a result of an interaction between the viral leader sequence and the viral nucleocapsid protein (63, 65). In SARS-CoV-infected cells, translation of the viral mRNAs is favored over cellular mRNAs in part by an endonucleoproteolytic property of viral nsp1, which cleaves the 5′-terminal sequence of cellular but not viral mRNAs (66–68). In this light, the mechanisms by which uORFs regulate resistance to the effect of cell stress in other cellular and viral mRNAs might be instructive for further studies on coronavirus translation regulation. For example, uORF translation enhances shunting in cellular mRNA cIAP2 (9), in prototype foamy virus genomic RNA (11), and in rice tungro virus (4), in a way that enables the mRNA or viral RNA to escape translation inhibition. uORF-enhanced scanning in Ebola virus RNA (5) and hepatitis B virus RNA (6) also enhances translation. However, none of these special mechanisms for translation of coronavirus nsp1 have yet been described.

ACKNOWLEDGMENTS

This work was supported by grant AI 14376 from the National Institutes of Health and in part by funds from the University of Tennessee, College of Veterinary Medicine, Center of Excellence Program for Livestock Diseases and Human Health.

REFERENCES

1. **Calvo SE, Pagliarini DJ, Mootha VK.** 2009. Upstream open reading frames cause widespread reduction of protein expression and are polymorphic among humans. Proc. Natl. Acad. Sci. U. S. A. **106:**7507–7512. http://dx.doi.org/10.1073/pnas.0810916106.
2. **Somers J, Poyry T, Willis AE.** 2013. A perspective on mammalian upstream open reading frame function. Int. J. Biochem. Cell Biol. **45:**1690–1700. http://dx.doi.org/10.1016/j.biocel.2013.04.020.
3. **Krummheuer J, Johnson AT, Hauber I, Kammler S, Anderson JL, Hauber J, Purcell DF, Schaal H.** 2007. A minimal uORF within the HIV-1 vpu leader allows efficient translation initiation at the downstream env

AUG. Virology **363:**261–271. http://dx.doi.org/10.1016/j.virol.2007.01.022.
4. **Pooggin MM, Rajeswaran R, Schepetilnikov MV, Ryabova LA.** 2012. Short ORF-dependent ribosome shunting operates in an RNA picorna-like virus and a DNA pararetrovirus that cause rice tungro disease. PLoS Pathog. **8:**e1002568. http://dx.doi.org/10.1371/journal.ppat.1002568.
5. **Shabman RS, Hoenen T, Groseth A, Jabado O, Binning JM, Amarasinghe GK, Feldmann H, Basler CF.** 2013. An upstream open reading frame modulates Ebola virus polymerase translation and virus replication. PLoS Pathog. **9:**e1003147. http://dx.doi.org/10.1371/journal.ppat.1003147.
6. **Kimbi GC, Kew MC, Kramvis A.** 2012. The effect of the G1888A mutation of subgenotype A1 of hepatitis B virus on the translation of the core protein. Virus Res. **163:**334–340. http://dx.doi.org/10.1016/j.virusres.2011.10.024.
7. **Hentze MW, Gebauer F, Preiss T.** 2007. cis-Regulatory sequences and trans-acting factors in translation control, p 269–295. *In* Matthews MB, Sonenberg N, Hershey JWB (ed), Translation control in biology and medicine. Cold Spring Harbor Laboratory Press, Cold Spring Harbor, NY.
8. **Jackson RJ, Kaminski A, Poyry TAA.** 2007. Coupled termination-reiniation events in mRNA translation, p 197–223. *In* Matthews MB, Sonenberg N, Hershey JWB (ed), Translation control in biology and medicine. Cold Spring Harbor Laboratory Press, Cold Spring Harbor, NY.
9. **Sherrill KW, Lloyd RE.** 2008. Translation of cIAP2 mRNA is mediated exclusively by a stress-modulated ribosome shunt. Mol. Cell. Biol. **28:**2011–2022. http://dx.doi.org/10.1128/MCB.01446-07.
10. **Bastide A, Karaa Z, Bornes S, Hieblot C, Lacazette E, Prats H, Touriol C.** 2008. An upstream open reading frame within an IRES controls expression of a specific VEGF-A isoform. Nucleic Acids Res. **36:**2434–2445. http://dx.doi.org/10.1093/nar/gkn093.
11. **Schepetilnikov M, Schott G, Katsarou K, Thiebeauld O, Keller M, Ryabova LA.** 2009. Molecular dissection of the prototype foamy virus (PFV) RNA 5′-UTR identifies essential elements of a ribosomal shunt. Nucleic Acids Res. **37:**5838–5847. http://dx.doi.org/10.1093/nar/gkp609.
12. **Petty IT, Edwards MC, Jackson AO.** 1990. Systemic movement of an RNA plant virus determined by a point substitution in a 5′ leader sequence. Proc. Natl. Acad. Sci. U. S. A. **87:**8894–8897. http://dx.doi.org/10.1073/pnas.87.22.8894.
13. **Archambault D, Kheyar A, de Vries AA, Rottier PJ.** 2006. The intraleader AUG nucleotide sequence context is important for equine arteritis virus replication. Virus Genes **33:**59–68. http://dx.doi.org/10.1007/s11262-005-0030-z.
14. **Molenkamp R, van Tol H, Rozier BC, van der Meer Y, Spaan WJ, Snijder EJ.** 2000. The arterivirus replicase is the only viral protein required for genome replication and subgenomic mRNA transcription. J. Gen. Virol. **81:**2491–2496. http://vir.sgmjournals.org/content/81/10/2491.long.
15. **Raman S, Bouma P, Williams GD, Brian DA.** 2003. Stem-loop III in the 5′ untranslated region is a cis-acting element in bovine coronavirus defective interfering RNA replication. J. Virol. **77:**6720–6730. http://dx.doi.org/10.1128/JVI.77.12.6720-6730.2003.
16. **Snijder EJ, Meulenberg JJ.** 1998. The molecular biology of arteriviruses. J. Gen. Virol. **79**(Part 5)**:**961–979.
17. **Brian DA, Baric RS.** 2005. Coronavirus genome structure and replication. Curr. Top. Microbiol. Immunol. **287:**1–30. http://dx.doi.org/10.1007/3-540-26765-4_1.
18. **Gorbalenya AE, Enjuanes L, Ziebuhr J, Snijder EJ.** 2006. Nidovirales: evolving the largest RNA virus genome. Virus Res. **117:**17–37. http://dx.doi.org/10.1016/j.virusres.2006.01.017.
19. **Bouvet M, Debarnot C, Imbert I, Selisko B, Snijder EJ, Canard B, Decroly E.** 2010. In vitro reconstitution of SARS-coronavirus mRNA cap methylation. PLoS Pathog. **6:**e1000863. http://dx.doi.org/10.1371/journal.ppat.1000863.
20. **Chen Y, Cai H, Pan J, Xiang N, Tien P, Ahola T, Guo D.** 2009. Functional screen reveals SARS coronavirus nonstructural protein nsp14 as a novel cap N7 methyltransferase. Proc. Natl. Acad. Sci. U. S. A. **106:**3484–3489. http://dx.doi.org/10.1073/pnas.0808790106.
21. **Decroly E, Imbert I, Coutard B, Bouvet M, Selisko B, Alvarez K, Gorbalenya AE, Snijder EJ, Canard B.** 2008. Coronavirus nonstructural protein 16 is a cap-0 binding enzyme possessing (nucleoside-2′O)-methyltransferase activity. J. Virol. **82:**8071–8084. http://dx.doi.org/10.1128/JVI.00407-08.
22. **Lugari A, Betzi S, Decroly E, Bonnaud E, Hermant A, Guillemot JC, Debarnot C, Borg JP, Bouvet M, Canard B, Morelli X, Lecine P.** 2010. Molecular mapping of the RNA cap 2′-O-methyltransferase activation interface between severe acute respiratory syndrome coronavirus nsp10 and nsp16. J. Biol. Chem. **285:**33230–33241. http://dx.doi.org/10.1074/jbc.M110.120014.
23. **Feder M, Pas J, Wyrwicz LS, Bujnicki JM.** 2003. Molecular phylogenetics of the RrmJ/fibrillarin superfamily of ribose 2′-O-methyltransferases. Gene **302:**129–138. http://dx.doi.org/10.1016/S0378-1119(02)01097-1.
24. **von Grotthuss M, Wyrwicz LS, Rychlewski L.** 2003. mRNA cap-1 methyltransferase in the SARS genome. Cell **113:**701–702. http://dx.doi.org/10.1016/S0092-8674(03)00424-0.
25. **Masters PS.** 2006. The molecular biology of coronaviruses. Adv. Virus Res. **66:**193–292. http://dx.doi.org/10.1016/S0065-3527(06)66005-3.
26. **Sawicki SG, Sawicki DL, Siddell SG.** 2007. A contemporary view of coronavirus transcription. J. Virol. **81:**20–29. http://dx.doi.org/10.1128/JVI.01358-06.
27. **van Marle G, Dobbe JC, Gultyaev AP, Luytjes W, Spaan WJ, Snijder EJ.** 1999. Arterivirus discontinuous mRNA transcription is guided by base pairing between sense and antisense transcription-regulating sequences. Proc. Natl. Acad. Sci. U. S. A. **96:**12056–12061. http://dx.doi.org/10.1073/pnas.96.21.12056.
28. **Wu HY, Ozdarendeli A, Brian DA.** 2006. Bovine coronavirus 5′-proximal genomic acceptor hotspot for discontinuous transcription is 65 nucleotides wide. J. Virol. **80:**2183–2193. http://dx.doi.org/10.1128/JVI.80.5.2183-2193.2006.
29. **Wu HY, Brian DA.** 2010. Subgenomic messenger RNA amplification in coronaviruses. Proc. Natl. Acad. Sci. U. S. A. **107:**12257–12262. http://dx.doi.org/10.1073/pnas.1000378107.
30. **Hofmann MA, Chang RY, Ku S, Brian DA.** 1993. Leader-mRNA junction sequences are unique for each subgenomic mRNA species in the bovine coronavirus and remain so throughout persistent infection. Virology **196:**163–171. http://dx.doi.org/10.1006/viro.1993.1464.
31. **Yang D, Liu P, Giedroc DP, Leibowitz J.** 2011. Mouse hepatitis virus stem-loop 4 functions as a spacer element required to drive subgenomic RNA synthesis. J. Virol. **85:**9199–9209. http://dx.doi.org/10.1128/JVI.05092-11.
32. **Yount B, Denison MR, Weiss SR, Baric RS.** 2002. Systematic assembly of a full-length infectious cDNA of mouse hepatitis virus strain A59. J. Virol. **76:**11065–11078. http://dx.doi.org/10.1128/JVI.76.21.11065-11078.2002.
33. **Hirano N, Fujiwara K, Matumoto M.** 1976. Mouse hepatitis virus (MHV-2). Plaque assay and propagation in mouse cell line DBT cells. Jpn. J. Microbiol. **20:**219–225.
34. **Gaertner DJ, Winograd DF, Compton SR, Paturzo FX, Smith AL.** 1993. Development and optimization of plaque assays for rat coronaviruses. J. Virol. Methods **43:**53–64. http://dx.doi.org/10.1016/0166-0934(93)90089-A.
35. **Chen W, Baric RS.** 1996. Molecular anatomy of mouse hepatitis virus persistence: coevolution of increased host cell resistance and virus virulence. J. Virol. **70:**3947–3960.
36. **Chen W, Madden VJ, Bagnell CR, Jr, Baric RS.** 1997. Host-derived intracellular immunization against mouse hepatitis virus infection. Virology **228:**318–332. http://dx.doi.org/10.1006/viro.1996.8402.
37. **Zuker M.** 2003. Mfold Web server for nucleic acid folding and hybridization prediction. Nucleic Acids Res. **31:**3406–3415. http://dx.doi.org/10.1093/nar/gkg595.
38. **Mathews DH, Sabina J, Zuker M, Turner DH.** 1999. Expanded sequence dependence of thermodynamic parameters improves prediction of RNA secondary structure. J. Mol. Biol. **288:**911–940. http://dx.doi.org/10.1006/jmbi.1999.2700.
39. **Guan BJ, Wu HY, Brian DA.** 2011. An optimal cis-replication stem-loop IV in the 5′ untranslated region of the mouse coronavirus genome extends 16 nucleotides into open reading frame 1. J. Virol. **85:**5593–5605. http://dx.doi.org/10.1128/JVI.00263-11.
40. **Guan BJ, Su YP, Wu HY, Brian DA.** 2012. Genetic evidence of a long-range RNA-RNA interaction between the genomic 5′ untranslated region and the nonstructural protein 1 coding region in murine and bovine coronaviruses. J. Virol. **86:**4631–4643. http://dx.doi.org/10.1128/JVI.06265-11.
41. **de Groot RJ, Baker SC, Baric RS, Brown CS, Drosten C, Enjuanes L, Fouchier RA, Galiano M, Gorbalenya AE, Memish ZA, Perlman S, Poon LL, Snijder EJ, Stephens GM, Woo PC, Zaki AM, Zambon M, Ziebuhr J.** 2013. Middle East respiratory syndrome coronavirus (MERS-CoV): announcement of the Coronavirus Study Group. J. Virol. **87:**7790–7792. http://dx.doi.org/10.1128/JVI.01244-13.

42. **Woo PC, Lau SK, Lam CS, Lau CC, Tsang AK, Lau JH, Bai R, Teng JL, Tsang CC, Wang M, Zheng BJ, Chan KH, Yuen KY.** 2012. Discovery of seven novel mammalian and avian coronaviruses in the genus Deltacoronavirus supports bat coronaviruses as the gene source of Alphacoronavirus and Betacoronavirus and avian coronaviruses as the gene source of Gammacoronavirus and Deltacoronavirus. J. Virol. **86:**3995–4008. http://dx.doi.org/10.1128/JVI.06540-11.
43. **Kozak M.** 1989. The scanning model for translation: an update. J. Cell Biol. **108:**229–241. http://dx.doi.org/10.1083/jcb.108.2.229.
44. **Peabody DS.** 1989. Translation initiation at non-AUG triplets in mammalian cells. J. Biol. Chem. **264:**5031–5035.
45. **Chen SC, Olsthoorn RC.** 2010. Group-specific structural features of the 5′-proximal sequences of coronavirus genomic RNAs. Virology **401:**29–41. http://dx.doi.org/10.1016/j.virol.2010.02.007.
46. **Makino S, Lai MM.** 1989. Evolution of the 5′-end of genomic RNA of murine coronaviruses during passages in vitro. Virology **169:**227–232. http://dx.doi.org/10.1016/0042-6822(89)90060-3.
47. **Wu HY, Guy JS, Yoo D, Vlasak R, Urbach E, Brian DA.** 2003. Common RNA replication signals exist among group 2 coronaviruses: evidence for in vivo recombination between animal and human coronavirus molecules. Virology **315:**174–183. http://dx.doi.org/10.1016/S0042-6822(03)00511-7.
48. **Lai MM, Stohlman SA.** 1981. Comparative analysis of RNA genomes of mouse hepatitis viruses. J. Virol. **38:**661–670.
49. **Cencic R, Desforges M, Hall DR, Kozakov D, Du Y, Min J, Dingledine R, Fu H, Vajda S, Talbot PJ, Pelletier J.** 2011. Blocking eIF4E-eIF4G interaction as a strategy to impair coronavirus replication. J. Virol. **85:**6381–6389. http://dx.doi.org/10.1128/JVI.00078-11.
50. **Ingolia NT, Lareau LF, Weissman JS.** 2011. Ribosome profiling of mouse embryonic stem cells reveals the complexity and dynamics of mammalian proteomes. Cell **147:**789–802. http://dx.doi.org/10.1016/j.cell.2011.10.002.
51. **Ivanov IP, Firth AE, Michel AM, Atkins JF, Baranov PV.** 2011. Identification of evolutionarily conserved non-AUG-initiated N-terminal extensions in human coding sequences. Nucleic Acids Res. **39:**4220–4234. http://dx.doi.org/10.1093/nar/gkr007.
52. **Starck SR, Jiang V, Pavon-Eternod M, Prasad S, McCarthy B, Pan T, Shastri N.** 2012. Leucine-tRNA initiates at CUG start codons for protein synthesis and presentation by MHC class I. Science **336:**1719–1723. http://dx.doi.org/10.1126/science.1220270.
53. **Firth AE, Brierley I.** 2012. Non-canonical translation in RNA viruses. J. Gen. Virol. **93:**1385–1409. http://dx.doi.org/10.1099/vir.0.042499-0.
54. **Florkiewicz RZ, Ahluwalia A, Sandor Z, Szabo S, Tarnawski AS.** 2011. Gastric mucosal injury activates bFGF gene expression and triggers preferential translation of high molecular weight bFGF isoforms through CUG-initiated, non-canonical codons. Biochem. Biophys. Res. Commun. **409:**494–499. http://dx.doi.org/10.1016/j.bbrc.2011.05.033.
55. **Kozak M.** 1989. Context effects and inefficient initiation at non-AUG codons in eucaryotic cell-free translation systems. Mol. Cell. Biol. **9:**5073–5080.
56. **Plant EP, Rakauskaite R, Taylor DR, Dinman JD.** 2010. Achieving a golden mean: mechanisms by which coronaviruses ensure synthesis of the correct stoichiometric ratios of viral proteins. J. Virol. **84:**4330–4340. http://dx.doi.org/10.1128/JVI.02480-09.
57. **Brierley I, Boursnell ME, Binns MM, Bilimoria B, Blok VC, Brown TD, Inglis SC.** 1987. An efficient ribosomal frame-shifting signal in the polymerase-encoding region of the coronavirus IBV. EMBO J. **6:**3779–3785.
58. **Hofmann MA, Senanayake SD, Brian DA.** 1993. A translation-attenuating intraleader open reading frame is selected on coronavirus mRNAs during persistent infection. Proc. Natl. Acad. Sci. U. S. A. **90:**11733–11737. http://dx.doi.org/10.1073/pnas.90.24.11733.
59. **Chen W, Baric RS.** 1995. Function of a 5′-end genomic RNA mutation that evolves during persistent mouse hepatitis virus infection in vitro. J. Virol. **69:**7529–7540.
60. **Bechill J, Chen Z, Brewer JW, Baker SC.** 2008. Coronavirus infection modulates the unfolded protein response and mediates sustained translational repression. J. Virol. **82:**4492–4501. http://dx.doi.org/10.1128/JVI.00017-08.
61. **Hilton A, Mizzen L, MacIntyre G, Cheley S, Anderson R.** 1986. Translational control in murine hepatitis virus infection. J. Gen. Virol. **67**(Part 5)**:**923–932.
62. **Raaben M, Groot Koerkamp MJ, Rottier PJ, de Haan CA.** 2007. Mouse hepatitis coronavirus replication induces host translational shutoff and mRNA decay, with concomitant formation of stress granules and processing bodies. Cell. Microbiol. **9:**2218–2229. http://dx.doi.org/10.1111/j.1462-5822.2007.00951.x.
63. **Tahara SM, Dietlin TA, Bergmann CC, Nelson GW, Kyuwa S, Anthony RP, Stohlman SA.** 1994. Coronavirus translational regulation: leader affects mRNA efficiency. Virology **202:**621–630. http://dx.doi.org/10.1006/viro.1994.1383.
64. **Hershey JW, Sonenberg N, Mathews MB.** 2012. Principles of translational control: an overview. Cold Spring Harb. Perspect. Biol. **4:**a011528. http://dx.doi.org/10.1101/cshperspect.a011528.
65. **Nelson GW, Stohlman SA, Tahara SM.** 2000. High affinity interaction between nucleocapsid protein and leader/intergenic sequence of mouse hepatitis virus RNA. J. Gen. Virol. **81:**181–188. http://vir.sgmjournals.org/content/81/1/181.long.
66. **Huang C, Lokugamage KG, Rozovics JM, Narayanan K, Semler BL, Makino S.** 2011. SARS coronavirus nsp1 protein induces template-dependent endonucleolytic cleavage of mRNAs: viral mRNAs are resistant to nsp1-induced RNA cleavage. PLoS Pathog. **7:**e1002433. http://dx.doi.org/10.1371/journal.ppat.1002433.
67. **Kamitani W, Huang C, Narayanan K, Lokugamage KG, Makino S.** 2009. A two-pronged strategy to suppress host protein synthesis by SARS coronavirus Nsp1 protein. Nat. Struct. Mol. Biol. **16:**1134–1140. http://dx.doi.org/10.1038/nsmb.1680.
68. **Tanaka T, Kamitani W, DeDiego ML, Enjuanes L, Matsuura Y.** 2012. Severe acute respiratory syndrome coronavirus nsp1 facilitates efficient propagation in cells through a specific translational shutoff of host mRNA. J. Virol. **86:**11128–11137. http://dx.doi.org/10.1128/JVI.01700-12.